Hadamard-type Pulse-Phase Encoding for Imaging of Multi-resonant Fluorine-19 Nanoparticles in Targeted Molecular MRI

J. Keupp[1], S. A. Wickline[2], G. M. Lanza[2], and S. D. Caruthers[2]
[1]Philips Research Europe, Hamburg, Germany, [2]C-TRAIN, Washington University, St. Louis, Missouri, United States

Introduction

^{19}F-MRI [1] bears a high potential for molecular imaging allowing the direct quantification of nanoparticles (NP) [2] or fluorinated (anti-cancer) drugs [3]. Previously, $\alpha_v\beta_3$-integrin targeted NP have been shown to detect and quantify angiogenesis in tumor models [4, 5]. Towards human translation, clinically-relevant NP-substrates like perfluoro-octyl-bromide (PFOB) should be applied, but rich spectra and large chemical shifts (CS) add significant complexity (PFOB: 7 ^{19}F-resonances, 60 ppm). Many methods have been developed to manage CS-artifacts, but tradeoffs like long encoding time or a need for complex δB_0 and relaxation correction remain (IDEAL [6], echo-time encoding [7,8]). Herein, Hadamard encoding, known for slice encoding [9], is applied in the CS domain as a robust and efficient method to detect multi-resonant ^{19}F labels *in vitro* and *in vivo.*

Pulse-Phase Encoding (PPE)

Multi-band excitation pulses are used to simultaneously excite different CS components with arbitrary spacing and variable phase differences of $\pm\pi$. For the separation of N components, 2^{N-1} pulse variants are recorded (e.g. [+++];[++-];[+-+];[+--] for N=3). For reconstruction, phase variants are added and/or subtracted in the complex domain to yield separate CS components. These component images can be corrected for the (known) CS and combined for optimum SNR. This signal combination can improve overall scan efficiency, when the number of signal averages exceeds 2^{N-1}, as is typical for ^{19}F-MRI. Adding robustness, the relative phase between the encoding steps is effective during the RF excitation (t=0) and is preserved for any echo time or δB_0 frequency offset throughout the FOV. PPE can be applied for any MR sequence or trajectory, with reconstruction in k-space for non-cartesian cases.

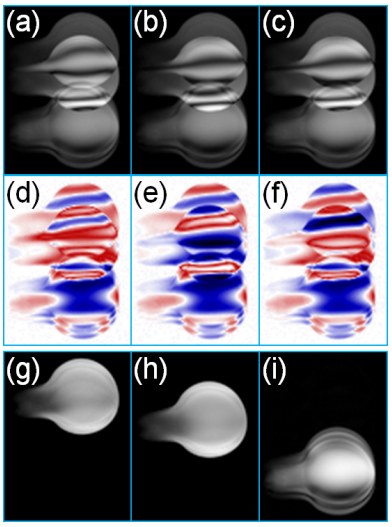

Figure 1: *In vitro* feasibility of pulse phase encoding in the CS domain under strong B_0 inhomogeneity (readout dir. bottom-top): 3 encoding steps with $\pm\pi$ phase variations (magnitude a,b,c; real part d,e,f) and clearly separated component images (g,h,i). Component (i) still comprises 5 resonances.

Experimental Methods

In this study, 3T clinical scanners (Achieva, Philips Healthcare, NL) and a ^{19}F/^{1}H transmit/receive surface coil were used. Modulated pulses were calculated within modified scanner software, and PPE was applied in a single examination loop.

(I) *In vitro*: A phantom (∅3cm) of pure PFOB was imaged: 3D GRE, TR/TE=12.7/7.4 ms, matrix 192×96×20, voxel 0.83×0.83×4 mm^3, center frequency on the PFOB-CF_2 line, doubly modulated Sinc-Gauss pulse, excitation bandwidth 4 kHz, α=50° (distributed over the multiple bands by modulation), modulations 4.8 kHz(CF_3) & 6.95 kHz(CFBr), 4 pulse phase variants, 2 min. scanning time.

(II) *In vivo*: New Zealand White rabbits (~2 kg, N=2) were implanted with Vx2 carcinoma (2-3 mm, hind leg), growing to ~15 mm in 2 weeks. 3h after injection (1.0 ml/kg) of $\alpha_v\beta_3$-targeted NP with PFOB core, the rabbits were anesthetized (xylazine/ketamine *i.m.* and 20 ml/h ketamine *i.v.* infusion) and imaged using a 3D dual-frequency [5] ^{19}F/^{1}H GRE sequence: 4 PPE-steps, voxel 5×5×4 mm^3, matrix 56×28×15, TR/TE=8.6/2.2 ms, α_{19F}/α_{1H}=75°/25°, pulse and modulation as in (I), modulation only on ^{19}F-pulse, 200 averages, scanning time 61 min. A calibration sample with PFOB-NP (150 mmol$_{19F}$/l) in agar was added. T1w-GRE images were recorded for anatomical co-registration (0.55×0.55×4.0 mm^3, TR/TE=24/6.5 ms, α=35°). All animal care and protocols were in accordance with institutional guidelines.

Results, Discussion

PPE imaging was successfully demonstrated *in vitro* (Fig.1). Under conditions of strong B_0 inhomogeneity, the CS artifact results in a complex superposition pattern which is varied in the consecutive PPE steps (3 out of 4 shown: Fig.1a,b,c), and the π-phase shifts are discernible in the real-part (Fig1.d,e,f:; red=pos., blue=neg.). In the PPE reconstruction, the PFOB-components CFBr (Fig.1g), CF_3 (1h) and CF_2 (1i), the latter consisting of 5 resonance lines, could be clearly separated with on average suppression of the other lines by 100:1. The *in vivo* experiment (Fig. 2) proved the capability to separate CS-components; visible in a slice containing the calibration sample (Fig.2a), with the PPE reconstructed CF_2 component in (2b) and complex sum of all PPE steps in (2c) visualizing the multiple CS components. NP signal from the bone marrow [5] is visible adjacent to the sample. ^{19}F signal from the tumor (Fig.2d,e,f; yellow ROI) was too weak to clearly exhibit all components (2f). Nevertheless, a PPE reconstruction of the CF_2 component (Fig.2e) shows less noise and background, such that signal around the tumor and from the epiphyseal heads (arrows) is more clearly visualized than in the uncorrected sum of all PPE steps (Fig.2f).

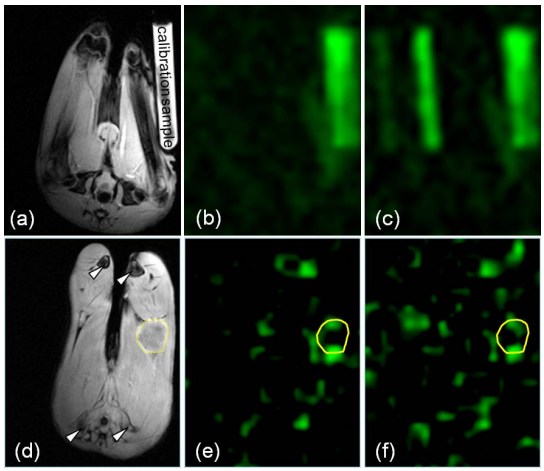

Figure 2: *In vivo* pulse-phase encoding applied to 3D ^{19}F molecular imaging of angiogenesis-targeted PFOB-NP on a Vx2 tumor (yellow ROI) in a rabbit leg: Selected slices containing bone/calibration sample (a,b,c) an the tumor (d,e,f). PPE of the PFOB-CF_2 component only (b,e) vs. all lines (c,f) demonstrates separation of chemical shift components (frequency encoding direction left- right).

Conclusion

A robust method to separate CS components of multi-resonant ^{19}F labels was implemented, and feasibility was demonstrated *in vitro* and *in vivo* for angiogenesis-targeted PFOB-NP in Vx2 tumor bearing rabbits.

References

1. Yu JX et al., Curr. Med. Chem. 12:819-848 (2005)
2. Morawski A et al., MRM 52:1255-1262 (2004)
3. Wolf W et al., Adv Drug Deliv Rev. 41:55-74 (2000)
4. Schmieder AH et al., FASEB J. 22(12):4179 (2008)
5. Keupp J et al., Proc. ISMRM 17:223 (2009)
6. Yu H et al., MRM 60(5):1122 (2008)
7. Posse S et al., Radiology 192:733-738 (1994)
8. Keupp J et al., Proc. ISMRM 14: 913 (2006)
9. Muller S., MRM 6:364 (1988)